Optical Multi-Tap RF Canceller for In-Band Full-Duplex Wireless Communication Systems

Yunlu Xing, Shangyuan Li, Xiaoxue Chen, Xiaoxiao Xue, and Xiaoping Zheng

***Abstract*—In-band full-duplex (IBFD) technology has become important for future wireless communications, due to its ability of increasing the radio-frequency (RF) spectrum efficiency. However, the benefits can only be realized if the self-interference (SI) is sufficiently suppressed. RF cancellation is important for IBFD systems due to its ability of SI mitigation. But it becomes more difficult for RF cancellation while the frequency and bandwidth increase. In real scenarios, the response of the multi-path SI channel is not frequency-flat, which also limits the cancellation performance. To solve these problems, we present a photonic-enabled multi-tap RF canceller in this paper. The proposed RF canceller has the ability of cancelling multi-path SI. The tap coefficients are precisely adjusted by optical spectrum processing. A prototype system with 8 taps is demonstrated in this paper. The measured results show 25 dB average cancellation depth over 1 GHz cancellation bandwidth under over-the-air conditions. To verify the signal of interest (SOI) recovery capability of the novel RF canceller, an IBFD wireless communication experiment based on 16-quadrature amplitude modulation (16-QAM) was demonstrated, the SOI was successfully recovered.**

***Index Terms*—Self-interference, RF cancellation, microwave photonics, in-band full-duplex.**

I. Introduction

IN-BAND full-duplex (IBFD) wireless communication systems doubles spectrum utilization by allowing the users to simultaneously occupy the same frequency band instead of using different time slots or different bands [1]. With the ability of transmitting and receiving on the same band and at the same time, IBFD technology facilitates several novel applications. IBFD systems have been studied for tactical communications and electronic warfare schemes due to its ability of providing physical-layer security and jamming enemy's receivers [2], [3]. IBFD technology also promotes cognitive radio technology, due to its capability of allowing users to simultaneously transmit and sense the spectrum [4]. However, the benefits mentioned above only become possible if the strong self-interference (SI) is sufficiently suppressed.

Partial transmitting signal leakages to the receiver may cause severe SI. The SI signal may reduce the dynamic range of the system and deteriorate receiver sensitivity. The SI cannot be mitigated by using notch filter or band-pass filter due to the band superposition of signal of interest (SOI) and SI.

To deal with this problem, the SI cancellation technology has been widely investigated. SI cancellation is typically conducted in three stages, including propagation domain suppression [5], [6], RF cancellation [7], [8] and digital cancellation [9], [10]. RF cancellation is of great important due to its ability of mitigating the SI before receiving and avoiding distortion. Traditional RF SI cancellation schemes based on electronic components have been widely investigated [11]. However, due to the electric bottleneck, the operating frequency and bandwidth of RF SI cancellation systems are limited. Compared to the traditional electronic RF cancellation schemes, the photonic-enabled RF cancellation technologies have the advantages of large bandwidth, high tuning precision and flat response, which can overcome the limitations of traditional electronic RF cancellers.

As summarized in [12], the incorporation of microwave-photonic technologies into RF SI cancellation systems effectively increase the operational bandwidth and cancellation depth. The photonic-enabled RF cancellation schemes can be time-domain focused or digitally assisted. To realize cancellation, the first type of cancellers precisely adjusts the frequency response of the canceller to make it opposite to the SI channel frequency response. Then, a small amount of original transmitting signal is coupled off before the antenna to serve as the reference signal. After processing in the optical domain, the reference signal is well-matched to SI signal and subtract it. Schemes have previously been proposed with direct laser modulation [13], [14], external optical intensity modulation [15], [16], [17], [18], [19], [20], [21], external polarization modulation [22], [23], and phase modulation [24], [25].

The majority of these schemes have only a few optical taps, which limits their performance under realistic over-the-air conditions. These schemes can only deal with the unrealistic situation that the response of SI channel is frequency-flat. Their ability of cancelling multi-path SI signal is also limited by the modest tap counts. The exception to that is the twenty-tap system in [25]. The cancellation depth of 20 dB over 1 GHz bandwidth and 25 dB over 500 MHz were achieved. However, due to the limited operating bandwidth and the imbalance between two outputs of the hybrid coupler, the cancellation performance is poor while cancelling high frequency and broadband SI signal. The tap delays are difficult to tune which also limits the cancellation performance.

Manuscript received 12 July 2022; accepted 15 September 2022. Date of publication 19 September 2022; date of current version 29 September 2022. This work was supported by the National Key Research and Development Program of China under Grant 2019YFB2203301. *(Corresponding author: Xiaoping Zheng.)*

The authors are with the Tsinghua National Laboratory for Information Science and Technology, Department of Electronic Engineering, Tsinghua University, Beijing 100084, China (e-mail: xingyl20@mails.tsinghua.edu.cn; syli@mail.tsinghua.edu.cn; chenxx17@mails.tsinghua.edu.cn; xuexx@tsinghua.edu.cn; xpzheng@mail.tsinghua.edu.cn).

Digital Object Identifier 10.1109/JPHOT.2022.3207787

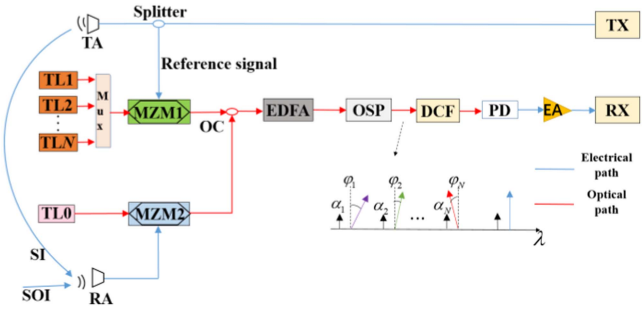

Fig. 1. Architecture of the proposed multi-tap RF canceller. RA, receiving antenna; TA, transmitting antenna; TL, tunable laser; Mux, multiplexer; MZM, Mach-Zehnder modulator; DCF, dispersion compensation fiber; OC, optical coupler; OSP, optical spectrum processer; EDFA, erbium-doped fiber amplifier; EA, electrical amplifier; PD, photodetector; RX, receiver; TX, transmitter; SOI, signal-of-interest; SI, self-interference.

The digitally assisted schemes directly cancel the SI signal by utilizing an auxiliary transmit channel [27], [28], [29], [30]. These schemes can provide a significantly higher number of adaptive taps, which are realized in digital domain. Thanks to its high flexibility, the digital assisted canceller can effectively cancel multi-path SI signal. In [30], a digital-assisted multi-path photonic SI cancellation and frequency down-conversion method was proposed, more than 26 dB cancellation depth of QPSK-modulated signal with the baud rate up to 1Gbaud has been achieved. However, the auxiliary transmit channel may worsen receiver's sensitivity because of the additive noise. Besides, it cannot eliminate the noise and the nonlinear components of the SI signal because they are not captured.

In [31], we have proposed a photonic-enabled SI canceller based on optical spectrum processor, and the prototype with one canceller tap was experimentally demonstrated. A novel multi-tap RF canceller is further proposed in this paper, and is able to be scaled to more than 8 taps demonstrated. To realize high cancellation depth, the frequency response of the canceller is precisely adjusted by tuning the tap coefficients to make it opposite to SI channel frequency response. With this purpose, the reference signal is modulated to multi-wavelength optical carriers, the phase and amplitude of each optical signal are finely tuned by an optical spectrum processor (OSP). After processing, the reference signal is well-matched to SI signal, and the SI is cancelled after the two photocurrents are combined at a photodetector (PD). Measured results show 25 dB cancellation depth over 1 GHz cancellation bandwidth under over-the-air conditions. Besides, IBFD wireless communication experiment based on 16-QAM has also been demonstrated, the signal of interest (SOI) was recovered.

II. Principle

A. Description of the Architecture

The architecture of the proposed multi-tap RF canceller is shown in Fig. 1. A small amount of transmission signal is coupled off before the transmitting antenna to serve as the reference signal. Because the SI channel responses are not frequency-flat under over-the-air conditions, the adjustment of reference signal should be different with frequencies over the whole frequency band, which can be realized by the proposed multi-tap architecture.

The tunable lasers (TLs) were utilized to emit optical carriers with different wavelengths. The reference signal is modulated to MZM1, and the received signal is modulated to MZM2, respectively.

We firstly analyze the upper branch. Multi-wavelength optical carriers are coupled into one path, which can be expressed as

$$E_{C1}(t) = \sum_{n=1}^{N} \sqrt{p_n} \exp(j\omega_n t) \tag{1}$$

where p_n and ω_n are the optical intensity and angular frequency of the optical signals, N is the tap number. Assuming the transmission signal is $T(t) = V_1 \cos(\omega_r t)$, where V_1, ω_r are the amplitude and angular frequency of the transmitting signal. The reference signal can be seen as a copy of transmitting signal. Around the quadrature bias point, the optical fields at the output of MZM1 can be expressed as

$$E_{ref}(t) = \frac{\sqrt{2}}{2} E_{C1}(t) \left\{ \exp\left[j \frac{m_1}{2} \cos(\omega_r t) + j \frac{\pi}{2} \right] + \exp\left[-j \frac{m_1}{2} \cos(\omega_r t) \right] \right\} \tag{2}$$

where $m_1 = \pi V_1 / V_\pi$ is the modulation indices, V_π is the half-wave voltage of the MZM. Utilizing a small signal approximation, (2) can be rewritten as

$$E_{ref}(t) \propto \sum_{n=1}^{N} \sqrt{p_n} \begin{Bmatrix} J_0\left(\frac{m_1}{2}\right) \exp(j\omega_n t) \\ -J_1\left(\frac{m_1}{2}\right) \exp[j(\omega_n + \omega_r) t] \\ -J_1\left(\frac{m_1}{2}\right) \exp[j(\omega_n - \omega_r) t] \end{Bmatrix} \tag{3}$$

where J_n is the nth-order Bessel function of the first kind. The reference signal is then amplified by an erbium-doped fiber amplifier (EDFA) and be adjusted by the OSP. OSP suppresses the upper sideband of each optical signal, as well as adjusts the amplitudes of the lower sidebands and the phases of the optical carriers. It is worth noting that, we can also adjust the phases of the lower sidebands and the amplitudes of the optical carriers, or introduce the amplitude and phase coefficients in one of them, for example, the carrier. These methods are the same to control the amplitudes and phases of the optical signals. After optical signal processing, the reference signal can be written as

$$E_{ref}(t) \propto \sum_{n=1}^{N} \sqrt{p_n} \begin{Bmatrix} \alpha_n J_0\left(\frac{m_1}{2}\right) \exp(j\omega_n t) \\ -J_1\left(\frac{m_1}{2}\right) \exp[j(\omega_n + \omega_r) \\ t + j\varphi_n] \end{Bmatrix} \tag{4}$$

where α_n and φ_n are the amplitude and phase adjustment coefficients, respectively. Thanks to the sheer optical spectrum processing ability of liquid crystal on Silicon (LCoS) [32], the control of the amplitude and phase can be precise and flexible. The dispersion compensation fiber (DCF) is utilized to introduce the tap delay. After propagation through the DCF, the optical

field can be written as

$$E_{ref}(t) \propto \sum_{n=1}^{N} \sqrt{p_n} \exp(j\omega_n t) \times \left\{ \begin{array}{l} \alpha_n J_0\left(\frac{m_1}{2}\right) \exp\left[j\theta(\omega_n)\right] \\ -J_1\left(\frac{m_1}{2}\right) \exp\left[j\omega_r t + j\varphi_n + j\theta(\omega_n + \omega_r)\right] \end{array} \right\} \quad (5)$$

where $\theta(\omega)$ is an additional phase term added to the signal introduced by DCF, which can be expressed as

$$\theta(\omega) = \theta_0 + \theta_1(\omega - \omega_1) + \frac{\theta_2}{2}(\omega - \omega_1)^2 \quad (6)$$

where θ_0 is a constant of phase shift, θ_1 is the total group delay of DCF. θ_2 relates to the dispersion parameter D (in ps/nm/km) as

$$\theta_2 = \frac{D\lambda^2 L}{2\pi c} \quad (7)$$

where λ is the wavelength of the optical signal, L is the length of the DCF and c is the speed of the light.

The higher order dispersion is negligible. After transmitting through the DCF, a photodetector (PD) converts the optical signals to the RF domain. The output reference signal can be written as

$$I_{ref}(t) \propto \Re J_0\left(\frac{m_1}{2}\right) J_1\left(\frac{m_2}{2}\right) \times \sum_{n=1}^{N} \alpha_n p_n \cos\left[\omega_r(t + \theta_1 + \tau_n) + \varphi_n + \frac{\theta_2}{2}\omega_r^2\right] \quad (8)$$

where $\Re$ is the responsivity of the PD. The tap delay can be expressed as

$$\tau_n = \theta_2(\omega_n - \omega_1) \quad (9)$$

Therefore, the transfer function of the upper branch can be expressed as

$$H_1(\omega_r) \propto \Re \exp\left(j\theta_1\omega_r + j\frac{\theta_2}{2}\omega_r^2\right) \times \sum_{n=1}^{N} p_n \alpha_n \exp\left[j\omega_r\tau_n + j\varphi_n\right] \quad (10)$$

By taking an inverse Fourier transform of (10), we can write the time domain response function as

$$h_1(t) \propto \Re \sum_{n=1}^{N} p_n \alpha_n \exp\left[j\frac{(t + \tau_n + \theta_1)^2}{2\theta_2} + j\varphi_n\right] \quad (11)$$

Since the input reference signal shares the same source of transmitting signal, $I_{ref}(t)$ can be expressed as the convolution of $h_1(t)$ and $T(t)$.

The upper branch of the canceller can be considered as a N-tap finite-impulse-response (FIR) filter with complex coefficients. The arbitrary frequency response of upper branch can be achieved by finely tuning the tap coefficients. Therefore, the proposed cancellation scheme has the capability to cancel the self-interference signal even if the SI channel response is not frequency-flat.

The signal received at the receiving antenna (RA) can be expressed as

$$R(t) = h_{SI}(t) \otimes T(t) + y_{SOI}(t) \quad (12)$$

where $h_{SI}(t)$ is the impulse response of the self-interference channel, the operator '$\otimes$' represents convolution, $y_{SOI}(t)$ is SOI. The received signal is modulated to a single-wavelength optical carrier with MZM2. The optical signal is then amplified by an EDFA, then it's up sideband is filtered out by OSP to avoid dispersion power fading. Unlike the optical signals in upper branch, the amplitude and phase of the optical signal in lower branch are not changed, as shown in Fig. 1. After transmitting through the DCF, the optical signal is converted to RF signal by the PD. According to the analysis above, the frequency response of the lower branch can be written as

$$H_2(\omega_r) \propto \Re \exp\left(j\theta_1\omega_r + j\frac{\theta_2}{2}\omega_r^2\right) \times p_0 \exp\left[j\omega_r\theta_2(\omega_0 - \omega_1)\right] \quad (13)$$

where p_0 is the optical intensity and ω_0 is the angular frequency of the optical signal emitted by TL0. By taking an inverse Fourier transform of (13), the time domain response function of the lower branch can be expressed as:

$$h_2(t) \propto \Re p_{lower} \exp\left\{j\frac{\left[t + \theta_1 + \theta_2(\omega_{lower} - \omega_0)\right]^2}{2\theta_2}\right\} \quad (14)$$

After transmitting through the lower branch, the SI signal can be expressed as

$$y_{SI}(t) = T(t) \otimes h_{SI}(t) \otimes h_2(t) \quad (15)$$

The addition of $I_{ref}(t)$ and $y_{SI}(t)$ is realized at the PD.

Therefore, the conditions for cancellation can be found, which can be written as

$$h_1(t) + h_{SI}(t) \otimes h_2(t) = 0 \quad (16)$$

(16) can also be expressed in frequency domain:

$$H_1(\omega_r) + H_{SI}(\omega_r) H_2(\omega_r) = 0 \quad (17)$$

where $H_{SI}(\omega_r)$ is the frequency response of the SI channel. Therefore, the target frequency response of the upper branch can be expressed as

$$G(\omega_r) = -H_{SI}(\omega_r) H_2(\omega_r) \quad (18)$$

The tap coefficients should be precisely tuned to approach the target frequency response.

B. Tuning Algorithm

To approximate the target frequency response, a tuning algorithm is designed to find the optimal solution. The algorithm is necessary because of the large number of degrees of freedom which makes it difficult to find the optimal tap coefficients manually.

Firstly, we model the canceller with a complex N-by-M matrix. The elements of the matrix indicate the frequency response

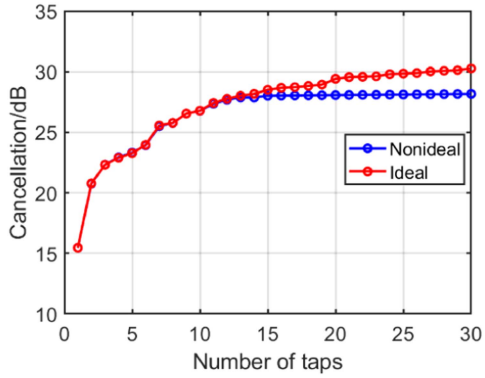

Fig. 2. RF cancellation depth with a varying number of taps under ideal and nonideal situation.

of each tap, which are measured while others are disabled. The matrix can be expressed as

$$\boldsymbol{H} = \begin{bmatrix} H_1(\omega_1) & H_1(\omega_2) & \cdots & H_1(\omega_M) \\ H_2(\omega_1) & H_2(\omega_1) & \cdots & H_2(\omega_M) \\ \vdots & \vdots & \ddots & \vdots \\ H_N(\omega_1) & H_N(\omega_2) & \cdots & H_N(\omega_M) \end{bmatrix} \tag{19}$$

where N is the total number of canceller taps, and M designates the number of samples for the cancellation bandwidth. The frequency response of the upper branch can be written as

$$\overrightarrow{\boldsymbol{H_1}} = \vec{\boldsymbol{w}} \cdot \boldsymbol{H} \tag{20}$$

where $\vec{\boldsymbol{w}}$ is the 1-by-N complex tap coefficient vector. Based on discrete mathematical model, the power of residual SI signal can be expressed as

$$\Delta P\left(\vec{\boldsymbol{w}}\right) = \left|\vec{\boldsymbol{G}} + \vec{\boldsymbol{w}} \cdot \boldsymbol{H}\right|^2 \tag{21}$$

where $\vec{\boldsymbol{G}}$ is a 1-by-M vector that represents the target frequency response. To minimize the power of the residual signal, we use CVX, which is a MATLAB-based modeling system for convex optimization, to find the optimal tap coefficients. The OSP is then programmed to realize cancellation.

C. Simulation Results

The system shown in Fig. 1 was simulated using a real-world SI channel, which was measured with a pair of K-band knife-edge antennas and a network analyzer. The simulation was focused on the SI between 18.0 and 19.0 GHz. In the simulation, we modeled the canceller as a FIR filter. The differential delay between taps was 0.5ns. With the tuning algorithm proposed in Section II-B, the simulation results are achieved.

Fig. 2 shows the RF cancellation depth with a varying number of taps under ideal and nonideal situation. The nonideal factor that affects the cancellation performance is OSP's maximum attenuation. The adjustment of tap coefficients is limited due to the OSP's maximum attenuation, which results in a limitation of cancellation depth. The typical attenuation limitation for a commercial waveshaper is 35 dB. Therefore, the maximum attenuation was set to be 35 dB in the simulation. As can be seen, the cancellation performance is strongly depended on the number of taps. The cancellation depth can be improved by adding more taps, within limits.

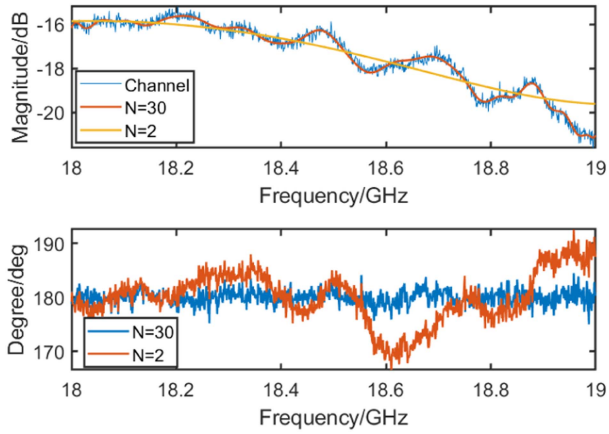

Fig. 3. Magnitude and phase offset of the SI channel response and simulated canceller responses of 2-tap and 30-tap canceller.

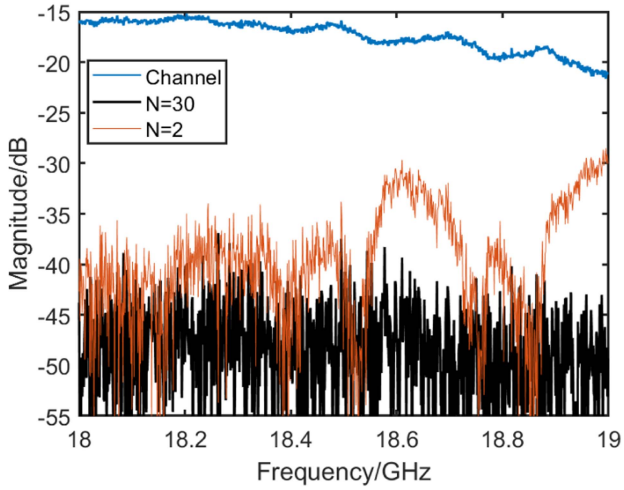

Fig. 4. Magnitude of SI channel response and simulated residual signals after cancellation of 2-tap and 30-tap canceller.

Fig. 3 shows the amplitude and phase responses of the canceller with 2 taps and 30 taps. It can be seen that the 30-tap canceller's magnitude response almost perfectly matches the SI channel magnitude response, and the phase response is nearly 180° offset. The 2-tap canceller's response cannot approach the SI channel response, which limits the cancellation performance.

Fig. 4 illustrates the simulated residual signals of combing the SI signal and the canceller output for both situations shown in Fig. 3. As can be seen, the 30-tap canceller provides higher cancellation depth, the power of residual signal is much lower.

III. Experimental Setup and Results

A. Over-the-Air Cancellation Performance

To evaluate the cancellation performance of the proposed scheme, an over-the-air cancellation experiment was conducted corresponding to Fig. 5. We used a Rohde & Schwarz's ZVA-67

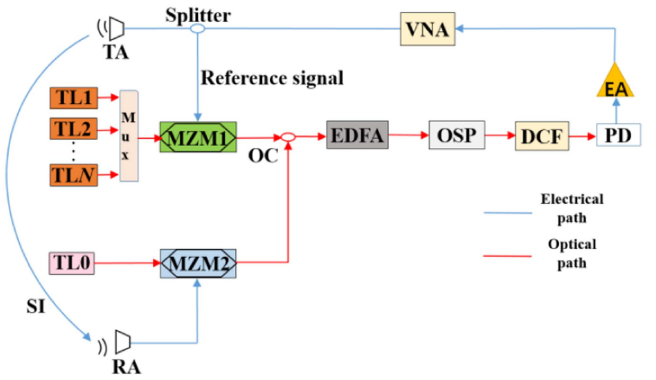

Fig. 5. The experimental setup to evaluate the cancellation performance. RA, receiving antenna; TA, transmitting antenna; TL, tunable laser; DCF dispersion compensation fiber; MZM, Mach-Zehnder modulator; EDFA, erbium-doped fiber amplifier; OSP, optical spectrum processor; EA, electronic amplifier; PD, photodetector; OC, optical coupler; VNA, vector network analyzer; SI, self-interference.

vector network analyzer (VNA) to emit broadband transmitting signal and measure the residual SI. The K-band antennas mentioned above were employed for over-the-air IBFD demonstration. A multi-channel laser (Anristu, MT9812B) was used as the multi-wavelength optical source. 8 optical signals were emitted which covered 193.8-195.2 THz with 200 GHz of spacing. The output power of each carrier was 6 dBm. TL0 was implemented by using a tunable semiconductor laser (TSL-550, Santec). The optical signals drove the MZMs (Fujitsu, FTM7938). The modulators have the half-voltage wave of 5 V and the 3-dB bandwidth of 37 GHz. The optical signals were then amplified by an EDFA. We used a waveshaper (Finisar, waveshaper 16000S) to process the optical signals. After processing in the optical domain, the signal went through the DCF with the dispersion of -320 ps/nm to introduce tap delay. Finally, the optical signals were converted back into RF domain via a PD (Finisar, MPRV1331A) with a bandwidth of 30 GHz and the SI was then cancelled.

The tap delay is 0.5ns in the experiment and simulation, and the maximum time delay difference of the 8-tap prototype system is 3.5ns. It is also possible to introduce time delay for paths with very long path difference. To achieve that, the frequency spacing of the optical carriers and the dispersion of the fiber should be very large according to (9). As discussed in [33], dispersion immunity is very important in application scenarios where fiber transmission is incorporated. To avoid dispersion power fading, the scheme removes the up sidebands of the optical signals by the OSP. Thus, this work is dispersion immunity even if the dispersion of the fiber is large.

The SI channel frequency response was firstly obtained by the VNA. The tuning algorithm described in the previous section was then utilized to configure the canceller's tap coefficients. The OSP was then programmed to mitigate SI. The simulation and experimental results of the 8-tap canceller are shown in Fig. 6(a) and (b), respectively. The SI was between 18.0 and 19.0 GHz. As can be seen, the canceller output is approximate to SI channel response. The simulated and experimental results showed 25.8 and 25.1 dB of average cancellation over the 1 GHz band in this instance.

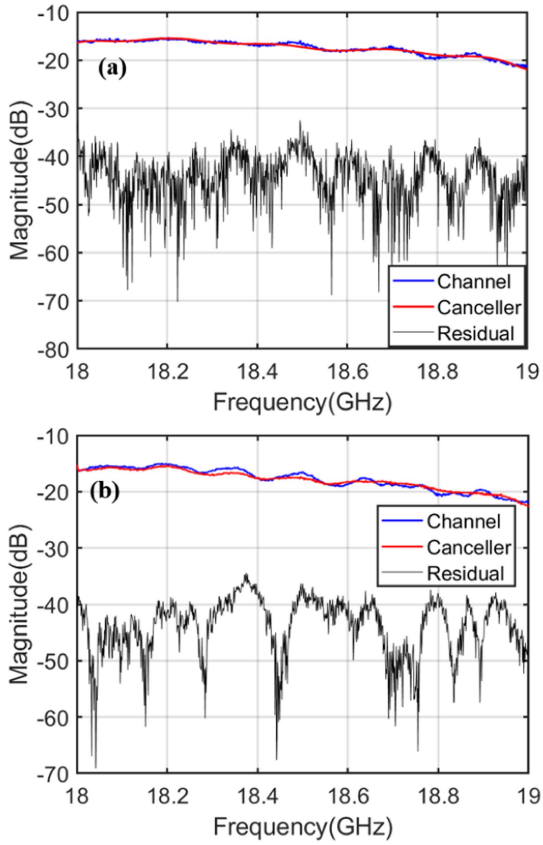

Fig. 6. (a) Simulation result and (b) experimental result of the 8-tap canceller output, SI channel response, and residual SI signal for 1 GHz bandwidth centered at 18.5 GHz.

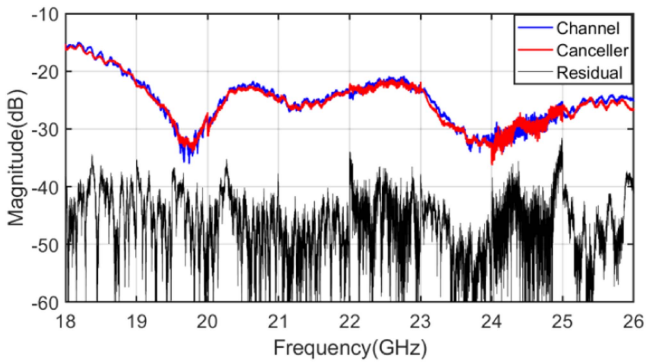

Fig. 7. Combined magnitude of canceller output, SI channel response, and residual SI signal for 1 GHz bandwidth tuned between 18 and 26 GHz.

Furthermore, the cancellation performances over different frequency bands were provided. Fig. 7 shows the cancellation performances over 1 GHz instantaneous bandwidth with different center frequencies. We tuned the RF canceller for eight times over the 8 GHz of bandwidth from 18 to 26 GHz (18 to 19, 19 to 20, 20 to 21, 21 to 22, 22 to 23, 23 to 24, 24 to 25 and 25 to 26). The results are combined into a single graphic. The measured average cancellation depth for these eight 1 GHz bands were 25.1, 16.7, 21.2, 23.6, 21.7, 20.1, 14.5 and 20.4 dB, respectively. The worst cancellation depth for these eight 1 GHz

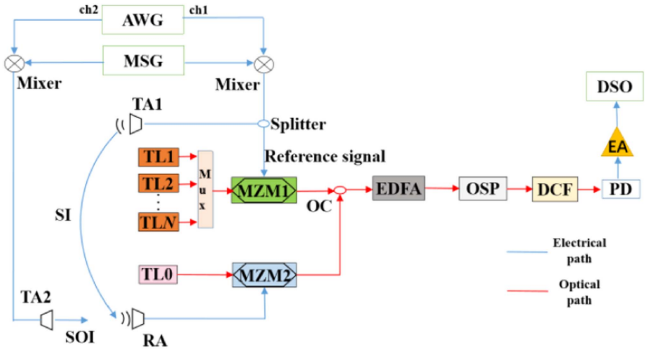

Fig. 8. The experimental setup to evaluate the SOI recovery capability. TL, tunable laser; DCF dispersion compensation fiber; MZM, Mach-Zehnder modulator; OC, optical coupler; OSP, optical spectrum processor; EDFA, erbium-doped fiber amplifier; EA, electronic amplifier; PD, photodetector; MSG, microwave signal generator; AWG, arbitrary waveform generator; ch1, channel 1; ch2 channel 2; DSO, digital signal oscilloscope; SOI, signal of interest; SI, self-interference; RA, receiving antenna; TA, transmitting antenna.

bands were 16.7 dB, 3.5 dB, 10.1 dB, 16.2 dB, 9.2 dB, 13.1 dB, 4 dB and 11.4 dB. As can be seen in Fig. 7, after cancellation, the magnitude of the residual signal is even over the whole frequency band. However, the magnitude of the interference is low in some bands, for example, 19 to 20 GHz and 24 to 25 GHz. Thus, the worst cancellation depth over the whole frequency band is low in some frequency bands. The experimental results show that, the canceller output is approximate to the SI channel response over the whole frequency band, even if the SI frequency band is not frequency-flat. The experimental results also indicate that the multi-tap scheme can mitigate multi-path SI signals.

In the experiment, the algorithm took about 0.85 s, and the CPU used for calculation is Intel(R) Core(TM) i5-10210U. The time for the commercial waveshaper to tune the tap coefficients is about 3 to 4 seconds. Therefore, if the SI channel response changes, the system has the ability of real-time reconstruction.

B. SOI Recovery

To evaluate the SOI recovery capability under over-the-air conditions, we built the experimental setup as shown in Fig. 8. We used a Tektronix's AWG70002A arbitrary waveform generator (AWG) to generate the baseband 16-QAM SOI and transmitting signal. We then used a microwave signal generator (MSG, Ceyear, 1465L-V) and mixers to up-convert the baseband signals. After finely adjusting the tap coefficients of the OSP, the SI was mitigated and the SOI was analyzed by using a digital signal oscilloscope (DSO).

Fig. 9 shows the SOI recovery performance with and without cancellation when a 16-QAM SOI with 200 MHz bandwidth and a SI signal with 1 GHz bandwidth centered at 18.5 GHz were used. Fig. 9(a) shows the output spectrum of SI and SOI signal with and without cancellation. As can be seen, the SI (blue curve) was efficiently suppressed and the SOI (orange curve) was successfully recovered. The average cancellation depth is about 21 dB. The constellation diagram was not clear without cancellation, as shown in Fig. 9(b). After cancellation, the SOI was well recovered with an error vector magnitude (EVM) of 9.34%, as shown in Fig. 9(c).

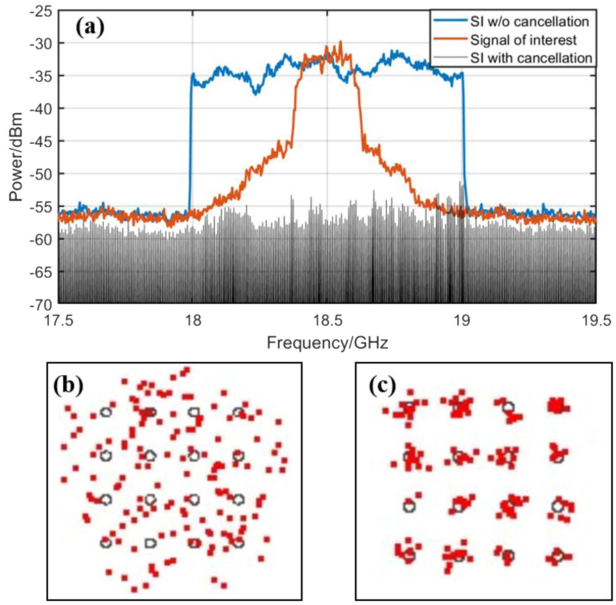

Fig. 9. SOI recovery performance when a 16-AQM SOI with 200 MHz bandwidth and a SI with 1 GHz bandwidth were used. (a) The measured spectrum of SI and SOI with and without cancellation. (b) The constellation diagram without cancellation. (c) The constellation diagram with cancellation.

The proposed multi-tap RF canceller has the capability to provide effective SI cancellation and SOI recovery under over-the-air conditions.

IV. Conclusion

A novel multi-tap RF canceller based on optical signal processing is proposed in this paper. Thanks to the considerable tap count, the proposed scheme provides high cancellation depth under over-the-air conditions. A tuning algorithm has been proposed to find the optimal tap coefficients. An 8-tap prototype system was experimentally demonstrated. The tap number can be easily scaled by adding additional optical carriers. Measured results show 25 dB cancellation depth over 1 GHz cancellation bandwidth under over-the-air conditions. Furthermore, under the interference of SI signal with 1 GHz bandwidth, a 16-QAM SOI with 200 MHz bandwidth was well-recovered with an EVM of 9.34%. Due to its capability of providing high cancellation depth under over-the-air conditions, the proposed multi-tap RF canceller has the potential to enable IBFD wireless communication systems.

References

[1] K. E. Kolodziej, B. T. Perry, and J. S. Herd, "In-band full-duplex technology: Techniques and systems survey," *IEEE Trans. Microw. Theory Techn.*, vol. 67, no. 7, pp. 3025–3041, Jul. 2019.

[2] T. Riihonen, D. Korpi, O. Rantula, H. Rantanen, T. Saarelainen, and M. Valkama, "Inband full-duplex radio transceivers: A paradigm shift in tactical communications and electronic warfare?," *IEEE Commun. Mag.*, vol. 55, no. 10, pp. 30–36, Oct. 2017.

[3] S. Talwar, D. Choudhury, K. Dimou, E. Aryafar, B. Bangerter, and K. Stewart, "Enabling technologies and architectures for 5G wireless," in *Proc. IEEE MTT-S Int. Microw. Symp. Dig.*, 2014, pp. 1–4.

[4] D. Cabric, S. Mishra, and R. Brodersen, "Implementation issues in spectrum sensing for cognitive radios," in *Proc. Asilomar Conf. Signals Syst. Comput.*, 2004, pp. 772–776.

[5] E. Everett, A. Sahai, and A. Sabharwal, "Passive self-interference suppression for full-duplex infrastructure nodes," *IEEE Trans. Wireless Commun.*, vol. 13, no. 2, pp. 680–694, Feb. 2014.
[6] G. Makar, N. Tran, and T. Karacolak, "A high-isolation monopole array with ring hybrid feeding structure for in-band full-duplex systems," *IEEE Antennas Wireless Propag. Lett.*, vol. 16, pp. 356–359, 2017.
[7] H. Krishnaswamy et al., "Full-duplex in a hand-held device—From fundamental physics to complex integrated circuits, systems and networks: An overview of the Columbia FlexICoN project," in *Proc. Asilomar Conf. Signals, Syst. Comput.*, 2016, pp. 1563–1567.
[8] H. Krishnaswamy and G. Zussman, "1 chip 2x the bandwidth," *IEEE Spectr.*, vol. 53, no. 7, pp. 38–54, Jul. 2016.
[9] M. Adams and V. K. Bhargava, "Use of the recursive least squares filter for self interference channel estimation," in *Proc. IEEE 84th Veh. Technol. Conf.*, 2016, pp. 1–4.
[10] D. Korpi, L. Anttila, V. Syrjala, and M. Valkama, "Widely linear digital self-interference cancellation in direct-conversion full-duplex transceiver," *IEEE J. Sel. Areas Commun.*, vol. 32, no. 9, pp. 1674–1687, Sep. 2014.
[11] C. D. Nwankwo, L. Zhang, A. Quddus, M. A. Imran, and R. Tafazolli, "A survey of self-interference management techniques for single frequency full duplex systems," *IEEE Access*, vol. 6, pp. 30242–30268, 2018.
[12] X. Han et al., "RF self-interference cancellation by using photonic technology," *Chin. Opt. Lett.*, vol. 19, no. 7, Jul. 2021, Art. no. 073901.
[13] J. J. Sun, M. P. Chang, and P. R. Prucnal, "Demonstration of over-the-air RF self-interference cancellation using an optical system," *IEEE Photon. Technol. Lett.*, vol. 29, no. 4, pp. 397–400, Feb. 2017.
[14] M. P. Chang, E. C. Blow, J. J. Sun, M. Z. Lu, and P. R. Prucnal, "Integrated microwave photonic circuit for self-interference cancellation," *IEEE Trans. Microw. Theory Techn.*, vol. 65, no. 11, pp. 4493–4501, Nov. 2017.
[15] J. Suarez, K. Kravtsov, and P. R. Prucnal, "Incoherent method of optical interference cancellation for radio-frequency communications," *IEEE J. Quantum Electron.*, vol. 45, no. 4, pp. 402–408, Apr. 2009.
[16] Y. Zhang, S. Xiao, H. Feng, L. Zhang, Z. Zhou, and W. Hu, "Self-interference cancellation using dual-drive Mach-Zehnder modulator for in-band full-duplex radio-over-fiber system," *Opt. Exp.*, vol. 23, no. 26, pp. 33205–33213, Dec. 2015.
[17] M. P. Chang, J. J. Sun, E. C. Blow, Y.-K. I. Iuang, and P. R. Prucnal, "A microwave photonic canceller for improved interference rejection in full duplex radio," in *Proc. IEEE Photon. Conf.*, 2016, pp. 493–494.
[18] Z. Tu, A. Wen, X. Li, and H. Zhang, "A photonic pre-distortion technique for RF self-interference cancellation," *IEEE Photon. Technol. Lett.*, vol. 30, no. 14, pp. 1297–1300, Jul. 2018.
[19] X. Li et al., "Optimized self-interference cancellation based on optical dual-parallel MZM for co-frequency and co-time full duplex wireless communication under nonlinear distortion and emulated multipath effect," *Opt. Exp.*, vol. 27, no. 26, pp. 37286–37297, 2019.
[20] D. Wang et al., "Photonics-assisted frequency conversion and self-interference cancellation for in-band full-duplex communication," *J. Lightw. Technol.*, vol. 40, no. 3, pp. 607–614, Feb. 2022.
[21] X. J. Fan, J. F. Du, G. Z. Li, M. Li, N. H. Zhu, and W. Li, "RF self-interference cancellation and frequency downconversion with immunity to power fading based on optoelectronic oscillation," *J. Lightw. Technol.*, vol. 40, no. 12, pp. 3614–3621, Jun. 2022.
[22] Y. Xiang, G. Li, and S. Pan, "Ultrawideband optical cancellation of RF interference with phase change," *Opt. Exp.*, vol. 25, no. 18, pp. 21259–21264, Sep. 2017.
[23] X. Hu, D. Zhu, L. Li, and S. Pan, "Photonics-based adaptive RF self-interference cancellation and frequency downconversion," *J. Lightw. Technol.*, vol. 40, no. 7, pp. 1989–1999, Apr. 2022.
[24] X. Han, B. Huo, Y. Shao, C. Wang, and M. Zhao, "RF self-interference cancellation using phase modulation and optical sideband filtering," *IEEE Photon. Technol. Lett.*, vol. 29, no. 11, pp. 917–920, Jun. 2017.
[25] X. Su et al., "Optical multipath RF self-interference cancellation based on phase modulation for full-duplex communication," *IEEE Photon. J.*, vol. 12, no. 4, Aug. 2020, Art. no. 7102114.
[26] K. E. Kolodziej, S. Yegnanarayanan, and B. T. Perry, "Photonic-enabled RF canceller for wideband in-band full-duplex wireless systems," *IEEE Trans. Microw. Theory Techn.*, vol. 67, no. 5, pp. 2076–2086, May 2019.
[27] Y. Zhang et al., "EML-based multi-path self-interference cancellation with adaptive frequency-domain pre-equalization," *IEEE Photon. Technol. Lett.*, vol. 30, no. 12, pp. 1103–1106, Jun. 2018.
[28] Y. Zhang, L. Li, S. Xiao, M. Bi, Y. Yu, and W. Hu, "Wideband over-the-air RF self-interference cancellation by an EML-based optical system with baseband predistortion," *IEEE Photon. J.*, vol. 9, no. 5, Oct. 2017, Art. no. 5503009.
[29] L. Zheng, Z. Liu, S. Xiao, M. P. Fok, Z. Zhang, and W. Hu, "Hybrid wideband multipath self-interference cancellation with an LMS pre-adaptive filter for in-band full-duplex OFDM signal transmission," *Opt. Lett.*, vol. 45, no. 23, pp. 6382–6385, Dec. 2020.
[30] M. Han, T. Shi, and Y. Chen, "Digital-assisted photonic analog wideband multipath self-interference cancellation," *IEEE Photon. Technol. Lett.*, vol. 34, no. 5, pp. 299–302, Mar. 2022.
[31] Y. Xing, S. Li, X. Xue, and X. Zheng, "Photonic-assisted RF self-interference cancellation based on optical spectrum processing," *J. Lightw. Technol.*, vol. 40, no. 7, pp. 2015–2022, Apr. 2022.
[32] G. Lazarev, P. J. Chen, J. Strauss, N. Fontaine, and A. Forbes, "Beyond the display: Phase-only liquid crystal on Silicon devices and their applications in photonics," *Opt. Exp.*, vol. 27, no. 11, pp. 16206–16249, May 2019.
[33] Y. Chen and S. Pan, "Simultaneous wideband radio-frequency self-interference cancellation and frequency downconversion for in-band full-duplex radio-over-fiber systems," *Opt. Lett.*, vol. 43, no. 13, pp. 3124–3127, 2018.